Journal of Power Sources, 43–44 (1993) 181–191

A model for the deliverable capacity of the TiS_2 electrode in a Li/TiS_2 cell

Z. Mao and R. E. White*

Center for Electrochemical Engineering, Department of Chemical Engineering, Texas A&M University, College Station, TX 77843 (USA)

Abstract

A mathematical model is presented for a Li/TiS_2 cell under galvanostatic discharge. This model has been used to illustrate the importance of considering the effect of the separator on the material utilization of a porous TiS_2 electrode in a Li/TiS_2 cell. The model predictions show that a porous TiS_2 electrode in a cell with a thin separator would deliver much more capacity than the electrode would in a large volume of electrolyte and that the material utilization of the TiS_2 electrode increases with a decrease in the separator thickness.

Introduction

Porous TiS_2 electrodes represent a class of insertion positive electrodes used in secondary Li batteries. To gain a better understanding of the transport processes in these electrodes during charge and discharge, West, Jacobsen, and Atlung developed a mathematical model for a cell with plane TiS_2 electrode [1] and a model for porous TiS_2 electrodes [2]. They found that electrolyte depletion in the electrode is the principal factor that limits the deliverable capacity of the porous electrode. They also showed how the deliverable capacity depends on electrode thickness, discharge current density, and on electrode porosity. Their model for porous TiS_2 electrodes with some extensions was used recently by Spotnitz *et al.* [3] to simulate the discharge behavior of Grace Li/TiS_2 cells. In these models, the concentrations of ionic species at the interface between the electrode and the separator were assumed to be a constant, which is equivalent to assuming that the electrode is immersed in a large volume of electrolyte. Theoretical predictions from such single electrode models would be useful for analyzing half-cell experimental data. However, for a Li/TiS_2 cell, the separator is quite thin (e.g., a typical thickness of the separator used in Li batteries is about 50 μm [4, 5]). When electrolyte depletion within the TiS_2 electrode occurs during discharge as predicted by these models, there must be a corresponding rise in the electrolyte concentration in the separator as required by the overall mass balance since the total amount of ionic species in the electrolyte phase must not change during discharge. This concentration rise in the separator may significantly affect the transport behavior of ionic species in the electrode. Therefore, in order to predict the discharge behavior of a TiS_2 electrode in a complete cell, the effect of the electrolyte in the separator on the performance of the TiS_2 electrode should be included in the mathematical analysis. In addition, it could be speculated that the charge and discharge

*Author to whom correspondence should be addressed.

0378-7753/93/$6.00

behavior of a porous TiS_2 electrode in a large volume of electrolyte would be significantly different from that of the electrode in a cell with a thin separator. A quantitative comparison of these differences may help battery designers and experimentlists in designing batteries and experiments with these electrodes.

The procedure for modeling a complete cell can be found in the mathematical models for similar systems such as $Li/SOCl_2$ [6, 7] and LiAl/FeS [8] cells. In this paper, the porous electrode model developed by West *et al.* [2] is reformulated for galvanostatic discharge and is extended to include a mass balance in the separator. The objective of this work is to illustrate the importance of the overall mass balance in predicting the deliverable capacity of the TiS_2 electrode.

Model equations

Since the purpose of this work is to investigate the effect of the electrolyte in the separator on the performance of the TiS_2 electrode, it is assumed here for simplicity that the electrolyte is an ideal binary solution consisting of Li^+, ClO_4^- ions and solvent. The mass balance equation for Li^+ ions in the electrolyte phase within the electrode includes migration and diffusion [2]:

$$\epsilon \frac{\partial C}{\partial t} = D_+ \frac{\partial^2 C}{\partial x^2} + D_+ \frac{F}{RT}\left(\frac{\partial C}{\partial x}\frac{\partial \phi}{\partial x} + C\frac{\partial^2 \phi}{\partial x^2}\right) + \frac{i_y g}{F} \tag{1}$$

where the symbol C represents the concentration of the electrolyte (either Li^+ or ClO_4^- ions), D_+ is the effective diffusion coefficient of Li^+ ions in the electrode, and ϵ represents the electrode porosity which is assumed to be a constant here. The other symbols in this equation have the same meanings as those used by West *et al.* [2] and are given in the list of symbols. The symbols g represents the specific surface area per unit volume of the electrode. If the solid phase is assumed to consist of numerous small cylindrical particles of equal length and radius (r), by neglecting the surface area of the ends of the cylindrical particles, g may be approximately expressed as:

$$g = 2(1-\epsilon)/r \tag{2}$$

In the electrolyte phase, the current is assumed to be carried by Li^+ and ClO_4^- ions only. Thus, the current density in the solution phase can be expressed in the terms of the flux of each ionic species [9]:

$$i = F(z_- N_- + z_+ N_+) = F\left(-D_+ \frac{\partial C}{\partial x} - D_+ \frac{F}{RT} C \frac{\partial \phi}{\partial x} + D_- \frac{\partial C}{\partial x} - D_- \frac{F}{RT} C \frac{\partial \phi}{\partial x}\right) \tag{3}$$

where z_- and z_+ are the charge numbers on Li^+ and ClO_4^- ions, and N_+ and N_- are the fluxes of Li^+ and ClO_4^- ions, respectively. A divergence of the current density in the electrolyte must be equal to the transfer current across the solid/electrolyte interface per unit volume of the electrode ($\nabla i = i_y g$), which yields a charge balance in the electrolyte:

$$F\left[(D_+ - D_-)\frac{\partial^2 C}{\partial x^2} + (D_+ + D_-)\frac{F}{RT}\left(\frac{\partial C}{\partial x}\frac{\partial \phi}{\partial x} + C\frac{\partial^2 \phi}{\partial x^2}\right)\right] + i_y g = 0 \tag{4}$$

where the term $i_y g$ represents the current per unit volume transferred from the electrolyte into the solid phase, and it is equal to the diffusion rate of the inserted

Li^+ ions into the bulk solid at the particle surface:

$$i_y = -FD_s\left(\frac{\partial C_s}{\partial y}\right)_{y=r} \tag{5}$$

where C_s and D_s represent the concentration of inserted Li^+ ions and its diffusion coefficient in the solid phase.

Equations (1) and (4) form a complete set of the equations needed to describe the electrolyte concentration and the potential in the electrolyte as a function of position and time. Their solution depends on the boundary conditions specified and on the transport behavior of inserted Li^+ ions in the solid phase. As shown in Fig. 1, at the current collector ($x=0$), the boundary conditions for C and ϕ can be easily specified as follows:

$$\left(\frac{\partial C}{\partial x}\right)_{x=0} = 0 \tag{6}$$

$$\left(\frac{\partial \phi}{\partial x}\right)_{x=0} = 0 \tag{7}$$

At the interface between the electrode and the separator ($x=L$), the current density in the electrolyte must be equal to be applied current density:

$$-F\left[(D_+ - D_-)\frac{\partial C}{\partial x} + \frac{F}{RT}(D_+ + D_-)C\frac{\partial \phi}{\partial x}\right]_{x=L} = i_{app} \tag{8}$$

and the continuity of concentration and flux across this interface should prevail, that is:

$$N_+|_{L^-} = N_+|_{L^+} \tag{9}$$

This boundary condition is referred here to as the flux boundary condition (FBC), as compared with the constant boundary condition (CBC) that was used by West *et al.* [2]

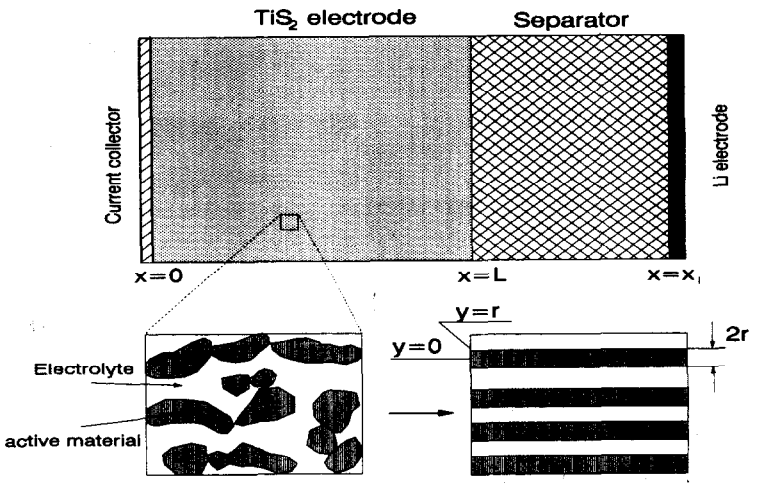

Fig. 1. A schematic of the model regions.

and Spotnitz *et al.* [3]:

$$C|_{x=L} = C_0 \tag{10}$$

The mass balance for the electrolyte in the separator is similar to eqn. (1) but without the term due to the charge transfer across the boundary between the solid and the electrolyte phases:

$$\epsilon_s \frac{\partial C}{\partial t} = D_+ \frac{\partial^2 C}{\partial x^2} + D_+ \frac{F}{RT} \frac{\partial}{\partial x} C \frac{\partial \phi}{\partial x} \tag{11}$$

Since the current density in the separator does not change, the product $C \frac{\partial \phi}{\partial x}$ in eqn. (11) can be substituted by $\frac{\partial C}{\partial x}$:

$$C \frac{\partial \phi}{\partial x} = -\frac{RT}{F^2} i_{app} - \frac{RT}{F} \frac{D_+ - D_-}{D_+ + D_-} \frac{\partial C}{\partial x} \tag{12}$$

Substitution of eqn. (12) into (11) yields the final mass balance for the electrolyte in the separator:

$$\epsilon_s \frac{\partial C}{\partial t} = \frac{2D_+ D_-}{D_+ + D_-} \frac{\partial^2 C}{\partial x^2} \tag{13}$$

At the Li electrode, the flux of Li^+ ions must be equal to the dissolution rate of Li and the flux of ClO_4^- ions is zero, which yields the boundary condition:

$$-2D_+ \left. \frac{\partial C}{\partial x} \right|_{x=x_1} = \frac{i_{app}}{F} \tag{14}$$

The Li^+ insertion process in the TiS_2 solid phase is described by Fick's diffusion law:

$$\frac{\partial C_s}{\partial t} = D_s \left(\frac{\partial^2 C_s}{\partial y^2} + \frac{1}{y} \frac{\partial C_s}{\partial y} \right) \tag{15}$$

At the center of cylindrical particles, the concentration gradient for the inserted Li^+ ions should be zero due to symmetry:

$$\left. \frac{\partial C_s}{\partial y} \right|_{y=0} = 0 \tag{16}$$

At the surface of solid TiS_2 particles (or the interface between the solid and the electrolyte) ($y=r$), the flux of inserted Li^+ ions into the bulk solid should be equal to the electrochemical reaction rate at the surface. For simplicity, it is assumed here that the kinetics of the electrochemical reaction is infinitely fast so that Li^+ ions in the electrolyte are in equilibrium with inserted Li^+ ions in the solid phase at the interface. A correlation between the two concentrations was given by West *et al.* [2]:

$$(\pi - \phi) = (\pi - \phi)_0 + \frac{RT}{F} \left(\ln \left(\frac{C_s^* - C_s}{C_s} \right) + \ln \frac{C}{C_0} - f \left(\frac{C_s}{C_s^*} - 0.5 \right) \right) \tag{17}$$

where π is the potential in the solid phase, which is assumed to be independent of the electrode position because of the high conductivity of the solid phase [2], C_s^*

represents the saturation concentration of inserted Li^+ ions in the solid phase, f is a constant, and $(\pi-\phi)_0$ is a constant.

Equations (1), (4), (13), and (15) with the boundary conditions specified by equations (6)–(9), (14), (16) and (17) form a complete set of the equations describing the electrolyte concentration, the potential in the electrolyte, and the concentration of inserted Li^+ ions in the solid phase as functions of position and time. To solve these equations, the initial conditions must be specified. The initial conditions used here are:

$$C = C_0 \text{ for all } x \tag{18}$$

$$C_s = C_s^0 \text{ for all } y \tag{19}$$

No initial conditions are needed for ϕ and π. Since π is independent of position, $(\pi-\phi)$ can be treated as one variable.

Numerical procedure

A finite difference method has been used to obtain the numerical solution in this work. The partial differential equations and the boundary conditions described above were first discretized using three-point central difference for both first and second derivatives and the Crank–Nicolson approximation to obtain accuracy on the order of (Δx^2) plus (Δt^2). The resulting nonlinear and coupled algebra equations were then solved using Newton–Raphson iteration method with the algorithm recently developed by Mao and White [10]. The input parameters are listed in Table 1, most of them are the same as those used by West *et al.* [2].

Results and discussion

Figure 2 presents a comparison of discharge curves for the two types of boundary conditions (FBC and CBC) described above. The state of discharge given in this Fig. was calculated using the equation:

$$\text{state of discharge} = \left(C_s^0/C_s^* + \frac{|i_{app}|t}{L(1-\epsilon)C_s^* F} \right) \times 100\%$$

As expected, the electrode potential decreases with the state of discharge. The constant boundary condition (CBC) results in both lower electrode potential and less deliverable capacity than the flux boundary condition. The decrease in the electrode potential is attributed to a decrease in the concentration of Li^+ ions in the electrolyte phase and to an increase in the concentration of inserted Li^+ ions in the solid phase at the solid/electrolyte interface, as indicated by eqn. (17). Under the simulation conditions given here, the concentration depletion for Li^+ ions in the electrolyte phase is the predominant factor in limiting the electrode capacity.

The concentration profiles for Li^+ ions in the electrolyte under the two-boundary conditions are shown in Figs. 3(a) and 3(b) at different states of discharge. Under the constant concentration boundary condition (Fig. 3(a)), the concentration of Li^+ ions decreases continuously in the electrode during the discharge and becomes nearly zero in the region toward the current collector at the end of discharge. Under the flux boundary condition (Fig. 3(b)), the concentration of Li^+ ions decreases only in

TABLE 1

Input parameters[a]

Symbol	Parameter
C_0	1.10×10^{-3} mol/cm^3
C_s^*	2.5×10^{-2} mol/cm^3
C_s^0	2.5×10^{-4} mol/cm^3
D_+^0	1.61×10^{-6} cm^2/s
D_-^0	6.45×10^{-6} cm^2/s
D_s	1.0×10^{-10} cm^2/s
F	96487 C/mol
f	16.2
g	2.6×10^4 cm^2/cm^3 (calculated using eqn. (2))
i_{app}	-5.0 mA/cm^2
L	0.05 cm
r	5.0×10^{-5} cm
R	8.314 J/(mol K)
T	298 K
δ	50.0×10^{-3} cm
ϵ	0.35
ϵ_s	0.55
$(\pi-\phi)_0$	2.17 V

[a] D_+ and D_- are calculated from D_i^0: $D_i=D_i^0\epsilon^{1.5}$ $(i=+,\ -)$ for the TiS_2 electrode and $D_i=D_i^0\epsilon_s^{1.5}$ $(i=+,\ -)$ for the separator.

the region near the current collector (not the entire electrode as in the CBC case), it increases rapidly in the region toward the separator. In this case, the concentration build-up in the region near the separator yields a higher driving force for diffusion of the ionic species into the electrode, and, consequently, delays the concentration depletion of Li^+ ions in the inner region. Figure 3(b) shows that the electrolyte concentration increases rapidly in the separator and becomes a linear function of position. Since this situation is more realistic in a cell during discharge than that predicted under the constant concentration boundary condition, it is necessary to include the effect of the electrolyte behavior in the separator in analyzing the performance of the TiS_2 electrode used in a Li/TiS_2 cell. However, it should be cautioned that the above predictions are for an ideal electrolyte where no chemical reaction in the electrolyte is considered. In an actual cell, the electrolyte concentration in the separator may reach its solubility limit and solid Li salt may precipitate out, preventing the electrolyte concentration from becoming higher and also possibly resulting in a passivation film on the Li electrode. A more realistic model would include both a mass balance for the entire cell and chemical reactions in the electrolyte as in the mathematical models for similar systems given in references [6–8].

Figures 4(a) and 4(b) present a comparison of the local transfer-current density as a function of electrode position for the two types of the boundary conditions. As expected from earlier discussions about the concentration profiles, charge is transferred from the electrolyte into the solid phase predominantly in the first half of the electrode toward the separator under the constant concentration boundary condition because Li^+ ions are available only in this region. It should be noted that at initial state of discharge Li^+ ions in the region near the current collector actually diffuse toward the region near the separator where they are transferred into the solid phase. Therefore,

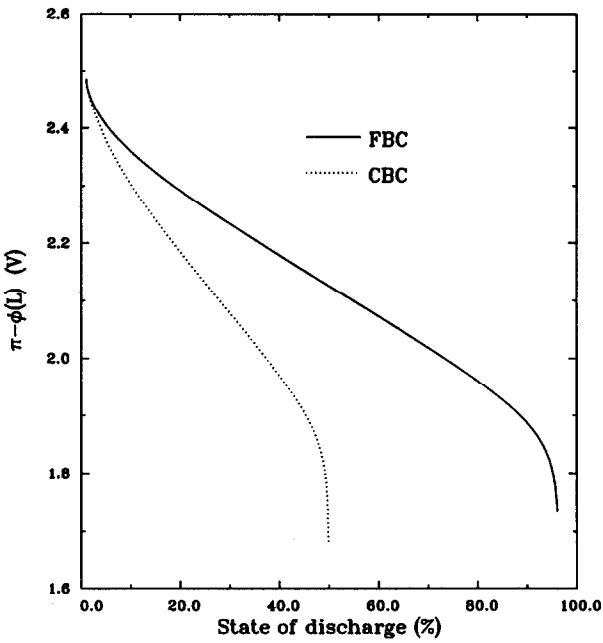

Fig. 2. A comparison of predicted discharge curves for the two different boundary conditions (FBC and CBC), where FBC represents flux boundary condition and CBC represents constant concentration condition.

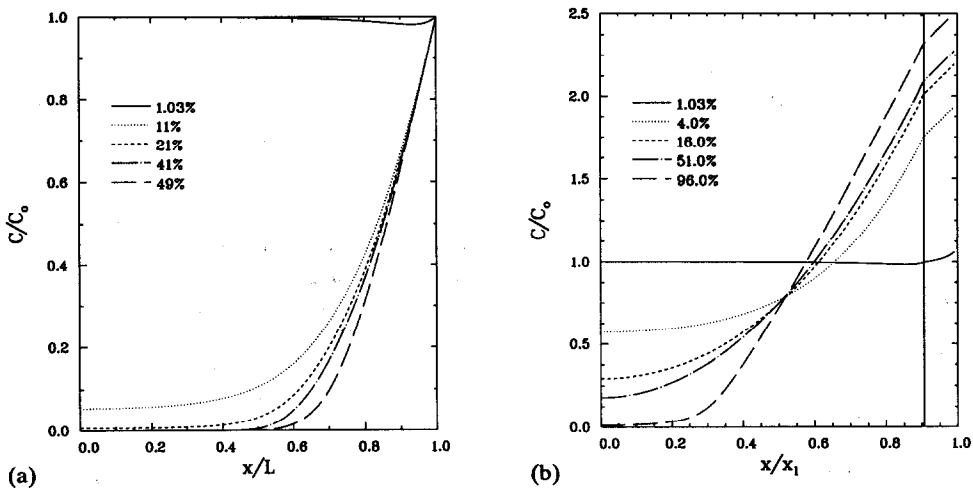

Fig. 3. Predicted concentration profiles for Li^+ ions in the electrolyte phase at different percents of discharged capacity: (a) under the constant concentration boundary condition, and (b) under the flux boundary condition.

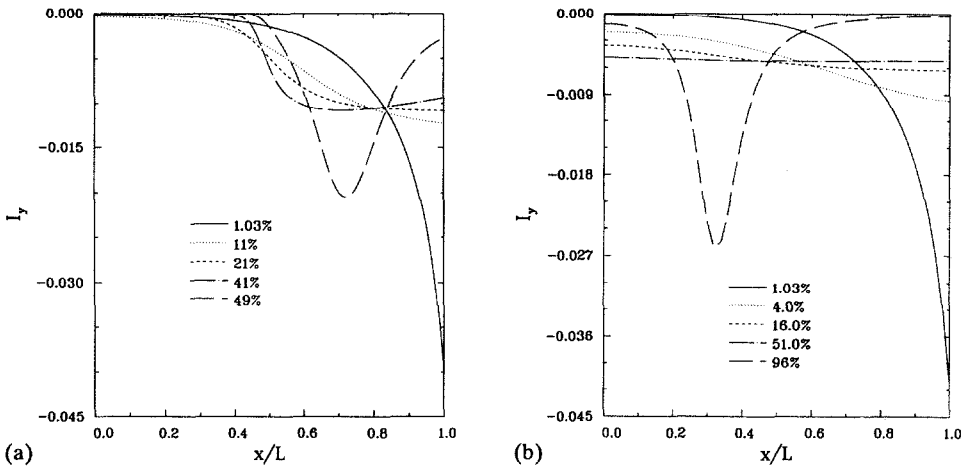

Fig. 4. Predicted dimensionless local transfer current density as a function of electrode position at different discharge states, where $I_y = -\frac{\Delta t}{C_0} D_s g\left(\frac{\partial C_s}{\partial y}\right)_{y=r}$, $\Delta t = 5$ s: (a) under the constant concentration boundary condition, and (b) under the flux boundary condition.

the concentration of Li^+ ions is rapidly depleted in the inner electrode. Although the initial transfer-current density predicted under the flux boundary condition has almost the same distribution as that predicted under the constant concentration boundary condition, the former gradually penetrates into the bulk electrode. When the solid phase near the separator becomes more and more saturated with the inserted Li^+ ions, the transfer current in this region becomes smaller and smaller, and the distance for Li^+ ions to diffuse to the reaction sites also becomes longer. Consequently, the charge transfer occurs in a narrowing region where the solid phase is not saturated with the inserted Li^+ ions and Li^+ ions are also available in the electrolyte phase.

Figures 5(a) and 5(b) present the concentration distributions for inserted Li^+ ions in the solid phase at the end of discharge (49% for CBC and 96% for FBC). It can be seen that the distribution in the solid phase (in the y direction) is quite uniform for both cases, indicating that the diffusion of inserted Li^+ ions in the solid phase is relatively fast, and is not the limiting factor for the potential drop under the given condition. However, this situation would change if the discharge-current density and the size of TiS_2 particles are increased. In the x direction the concentration distributions are highly nonuniform, particularly that predicted under the constant concentration boundary condition. Evidently, the nonuniform distribution is due to the concentration depletion of Li^+ ions in the electrolyte in the x direction. Therefore, it can be easily inferred that any means which can enhance mass transport in the electrolyte phase would improve the performance of the electrode. Obvious methods for this include increasing the electrolyte concentration and using thin, highly porous electrodes.

It can also be easily deduced from the analysis presented above that a thinner separator would result in an higher deliverable capacity for the electrode since the electrolyte concentration in the electrode near the separator would be higher for a thin separator than that for a thick separator. Figure 6 shows the effect of the separator thickness on the discharge curve. It can be seen that the deliverable capacity decreases

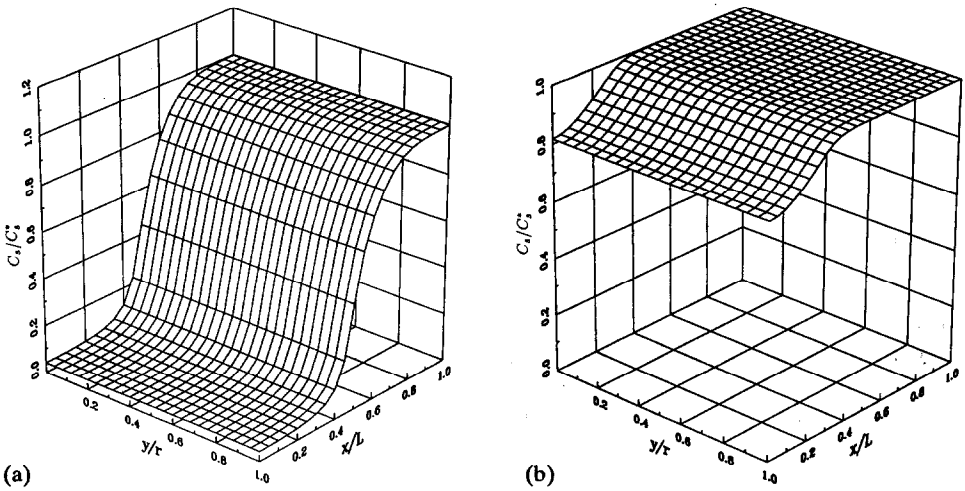

Fig. 5. Predicted dimensionless concentration profiles for inserted Li^+ ions in solid phase: (a) under the constant concentration boundary condition at the discharge state of 49%, and (b) under the flux boundary condition at the discharge state of 96%.

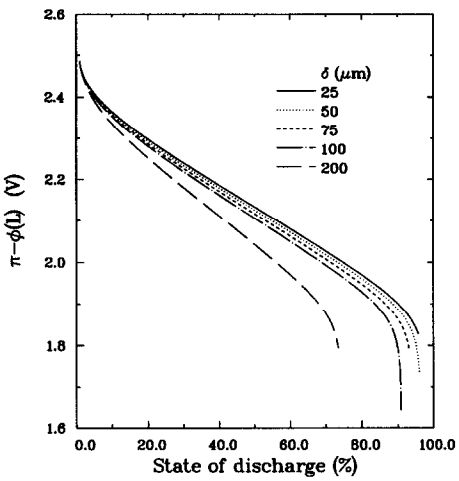

Fig. 6. Dependence of the discharge behavior on the separator thickness predicted under the flux boundary condition.

with an increase in the separator thickness. The discharge curves predicted with the flux boundary condition should become the same as those predicted with the constant concentration boundary condition when the electrolyte volume in the separator is essentially infinitely large compared to that in the electrode.

Conclusion

The mathematical model for porous TiS_2 electrodes developed by West *et al.* [2] has been reformulated for galvanostatic discharge and has been extended to include

the effect of the electrolyte in the separator. It has been shown that a TiS_2 electrode in a cell with a thin separator would deliver a much higher capacity than the same electrode would in a large volume of electrolyte and that use of a thinner separator would result in a considerable increase in the deliverable capacity of the electrode. In order to predict realistically the performance of the electrode as a function of design parameters, the effect of the electrolyte in the separator should be included.

Acknowledgements

This work was sponsored by Hughes Aircraft Company and by the Center for Space Power at Texas A&M University. Their financial support is gratefully acknowledged. Informative discussions with Mr Ricardo Prieto of our Center are appreciated. The authors are also very grateful for the computer time on the Cray-YMP supercomputer at Texas A&M University from Cray Research Inc.

List of symbols

C	concentration of Li^+ ions, mol/cm^3
C_0	initial concentration of Li^+ ions, mol/cm^3
C_s	concentration of inserted Li^+ ions in solid phase, mol/cm^3
C_s^*	saturation concentration of inserted Li^+ ions in solid phase, mol/cm^3
C_s^0	initial concentration of inserted Li^+ ions in solid phase, mol/cm^3
D_+	effective diffusion coefficient of Li^+ ions in the porous electrode or in the separator, cm^2/s
D_+^0	diffusion coefficient of Li^+ ions in free electrolyte, cm^2/s
D_-	effective diffusion coefficient of ClO_4^- ions in the porous electrode or in the separator, cm^2/s
D_-^0	diffusion coefficient of ClO_4^- ions in electrolyte, cm^2/s
D_s	diffusion coefficient of inserted Li^+ ions in solid phase, cm^2/s
F	Faraday's constant, 96487 C/mol
f	constant in eqn. (13)
g	specific surface area per unit volume, cm^{-1}
i	current density in electrolyte phase, A/cm^2
i_{app}	discharge current density, A/cm^2
i_y	local transfer-current density across electrolyte/solid interface, A/cm^2
I_y	$= -\frac{\Delta t}{C_0} D_s g \left(\frac{\partial C_s}{\partial y}\right)_{y=r}$, dimensionless local transfer-current density
L	electrode thickness, cm
R	universal gas constant, 8.3143 J/(mol K)
r	radius of cylindrical electrode particles, cm
T	temperature, K
t	time, s
x	spatial coordinate in electrolyte, cm
y	spatial coordinate in solid phase, cm
δ	separator thickness, cm
Δt	time step, s
ϵ	electrode porosity

ϵ_s	separator porosity
ϕ	potential in electrolyte phase, V
π	potential in solid phase, V

References

1 S. Atlung, K. West and T. Jacobsen, *J. Electrochem. Soc., 126* (1979) 1311–1321.
2 K. West, T. Jacobsen and S. Atlung, *J. Electrochem. Soc., 129* (1982) 1480–1485.
3 R. M. Spotnitz, D. Zuckerbrod, S. L. Johnson, J. T. Lundquist and R. E. White, R. E. White, M. W. Verbrugge and J. F. Stockel (eds.), *Proc. Symp. Modeling of Batteries and Fuel Cells,* The Electrochemical Society, Pennington, NJ, 1991, pp. 88–95.
4 K. W. Beard, *Proc. 34th Int. Power Sources Symp., Cherry Hill, NJ, USA, June 25–28, 1990,* Institute of Electrical and Electronics Engineers, Inc., pp. 160–163.
5 F. Walsh, *Proc. 34th Int. Power Sources Symp., Cherry Hill, NJ, USA, June 25–28, 1990,* Institute of Electrical and Electronics Engineers, Inc., pp. 164–166.
6 T. I. Evans, T. V. Nguyen and R. E. White, *J. Electrochem. Soc., 136* (1989) 328–338.
7 K. C. Tsaur and R. Pollard, *J. Electrochem. Soc., 131* (1984) 984–990.
8 R. Pollard and J. Newman, *J. Electrochem. Soc., 128* (1981) 491–502.
9 J. S. Newman (ed.), *Electrochemical Systems,* Prentice-Hall, Englewood Cliffs, NJ, 2nd edn., 1991, pp. 335–338.
10 Z. Mao and R. E. White, unpublished data.